Coupled Torsional and Longitudinal Vibrations of Piezoelectric Fiber Actuator With Helical Electrodes

Cheng Liang Pan, Zhi Hua Feng, Yu Ting Ma, Wei Wei Shao, and Yong Bin Liu

***Abstract*—The vibration characteristics of a piezoelectric fiber actuator with helical electrodes are studied theoretically and experimentally. Its working principle indicates that the torsional, longitudinal, and tangential deformations of the fiber are coupled. A simplified dynamic model is deduced to investigate the properties of the coupled vibrations and their corresponding equivalent circuits are also provided. Resonant frequencies and mechanical coupling coefficients in free-free boundary condition are calculated. The trends of resonant frequencies as functions of the electrode helical angle and fiber length are discussed and validated in experiments.**

I. Introduction

Piezoelectric elements are widely used in electromechanical devices as actuators and sensors to convert electrical signals into mechanical movements, and vice versa [1], [2]. The performances of these devices are usually dependent on the static and dynamic behaviors of piezoelectric elements and attached structures. Thus, analyses of the characteristics of piezoelectric elements are necessary for their successful applications in practical scientific and engineering problems.

Piezoelectric cylinders are important elements used for ultrasonic motors [3], [4], gyroscopes [5], [6], and acoustics devices [7], [8]. They are commonly designed with polarizing and driving electric field in the radial, longitudinal, and tangential (or circumferential) directions to actuate or sense bending, radial, longitudinal, torsional, and other vibrations [3]–[12]. Among these, torsional vibration is the most complicated one to achieve. Traditional ways of exciting torsional vibration include utilizing the d_{15} piezoelectric effect by assembling longitudinally polarized cylindrical sectors with a tangential driving electric field [10] or by stacking circumferentially polarized disks with a longitudinal driving electric field [11]. The electromechanical characteristics of these torsional elements have been presented in the literature [13], [14]. Another available way to generate torsional vibration is to polarize the piezoelectric cylinder helically with an angular deflection from the circumferential direction and excite it with a uniform longitudinal electric field [15]. However, this polarization is hard to achieve directly in practice.

In a past study, we presented a piezoelectric fiber actuator with the ability to generate torsional and longitudinal deformations simultaneously [16], which has been successfully used to supply vibrations for impact rotary motors [17] and optical scanning mirrors [18]. As shown in Fig. 1, with a pair of parallel electrode wires wound around its surface, forming a helical structure and likely interlacing similar to the interdigitated electrodes (IDEs) [19], [20], the fiber transforms into a torsional element. Piezoelectric fiber is actually a small cylinder and the torsional effect remains effective in large size [21]. A study of a similar tube piezoelectric transducer was reported by Xu *et al.* [22], who developed a 1-D mechanics model and gave numerical analyses of its vibration characteristics. In this study, an improved electromechanical model is created and experimental validation of the vibration characteristics of this kind of piezoelectric elements is conducted. First, working principle and static deformations of the fiber are explained briefly. Then, the dynamic model in the coupled vibrations is deduced and the corresponding equivalent circuits are provided. The trends of resonant frequencies and mechanical coupling coefficients are investigated with numerical analyses and validated in experiments.

II. Deformation of the Piezoelectric Fiber Actuator

Similar to the piezoelectric elements with IDEs, the induced electric field among the fibers is mainly perpendicular to the electrode lines and parallel to the outer surface of the fiber, which results in another helical route. Unlike the style used in [15], the helical direction of the electric field is reversed alternately when it traverses the helical electrodes and the polarizing and driving electric fields share the same electrodes. In the actuation state, the piezoelectric d_{33} coefficient induces an in-plane strain parallel to the electric field, whereas the d_{31} coefficient induces another in-plane strain perpendicularly. Both the d_{33} and d_{31} strains have nonzero shear and normal components in the longitudinal and tangential orthogonal coordinates of the fiber. These components result in the final torsional, longitudinal, and tangential deformations of the fiber. In the previous study [16], we analyzed the

Manuscript received January 25, 2011; accepted February 1, 2011. This work was partially supported by Project 50575216 from the National Natural Science Foundation of China.

C. L. Pan, Y. T. Ma, W. W. Shao, and Y. B. Liu are with the Department of Precision Machinery and Precision Instrumentation, University of Science and Technology of China, Hefei, Anhui, People's Republic of China.

Z. H. Feng is also with the Department of Precision Machinery and Precision Instrumentation, University of Science and Technology of China, Hefei, Anhui, People's Republic of China (e-mail: fff@ustc.edu.cn.)

Digital Object Identifier 10.1109/TUFFC.2011.1875

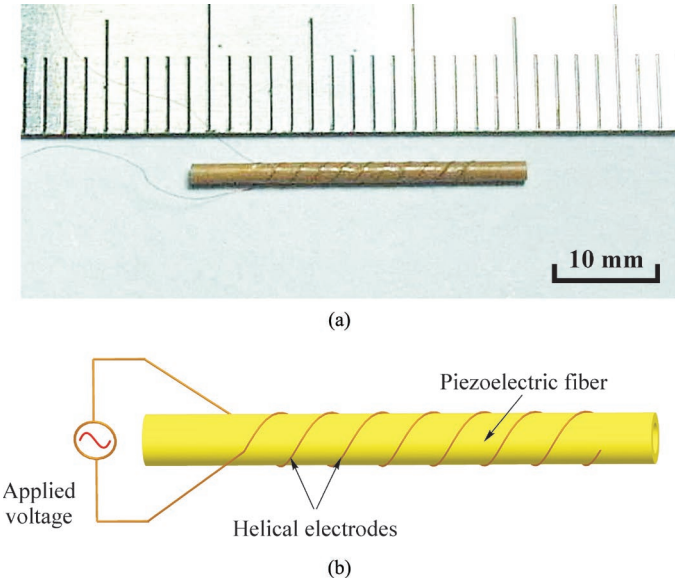

Fig. 1. A piezoelectric fiber actuator with helical electrodes: (a) photograph, (b) sketch.

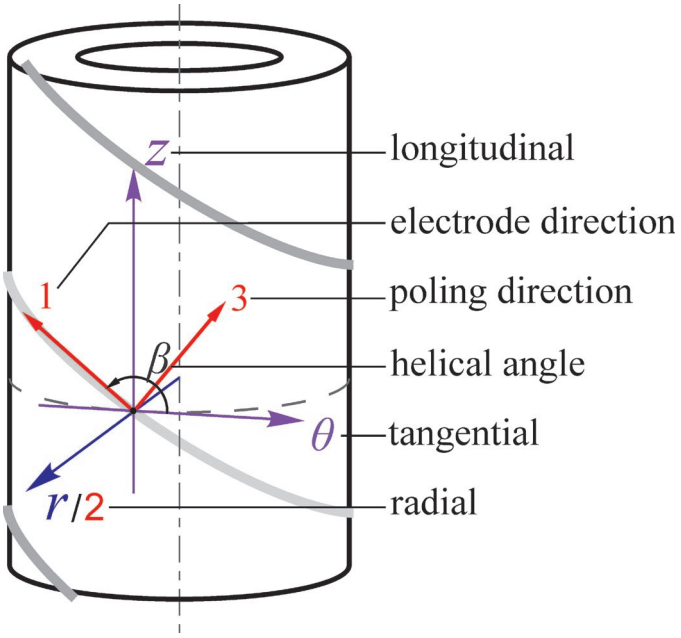

Fig. 2. Relationship between $r\theta z$ and 123 coordinates.

torsional and longitudinal strains of the fiber under static electric field in the free-load condition. The influences of the distribution of electric field, including its variations in the radial direction and non-uniformity between adjacent electrodes, on the performance of piezoelectric torsional displacement were discussed. Here, to simplify the process of dynamic analyses, the fiber is considered as a cylinder with thin wall thickness and uniform electric field, so the variations of relevant parameters in the radial and tangential directions are ignored.

As shown in Fig. 2, two coordinate systems are adopted to describe the electromechanical conversion of the fiber in formula, namely $r\theta z$ structure coordinates and 123 material coordinates. The r, θ, and z directions correspond to the radial, tangential, and longitudinal directions of the fiber. The 3 direction is the polarization direction, the 1 direction is parallel to the helical electrode lines, and the 2 direction is the same as the r direction. Meanwhile, l is the effective length of the fiber with electrodes, r_o is the outer radius, t is the wall thickness, p is the longitudinal distance between the adjacent electrodes (the helical pitch is defined as $2p$ for a fiber with one pair of electrodes), and β is the helical angle of electrodes.

The linear electromechanical relationships of piezoelectric material are typically characterized by piezoelectric equations in 123 coordinates:

$$\begin{pmatrix} \mathbf{S} \\ \mathbf{D} \end{pmatrix} = \begin{pmatrix} \mathbf{s}^{\mathrm{E}} & \tilde{\mathbf{d}} \\ \mathbf{d} & \boldsymbol{\varepsilon}^{\mathrm{T}} \end{pmatrix} \begin{pmatrix} \mathbf{T} \\ \mathbf{E} \end{pmatrix}, \tag{1}$$

where $\mathbf{S}$, $\mathbf{T}$, $\mathbf{E}$, and $\mathbf{D}$ are the matrices of strain, stress, electric field, and electric displacement, respectively. $\mathbf{s}^{\mathrm{E}}$, $\mathbf{d}$, and $\boldsymbol{\varepsilon}^{\mathrm{T}}$ are the matrices of elastic compliance coefficient, piezoelectric coefficient, and permittivity constant, respectively (superscripts E and T refer to the material constants determined with constant electric field and stress).

Although electric parameters are conveniently described in 123 coordinates, strains and stresses are more suitably defined in $r\theta z$ coordinates for the fiber. Thus, by substituting $S = AS'$ and $T = BT'$ in (1), the piezoelectric equations are transformed into a more appropriate form:

$$\begin{pmatrix} \mathbf{S}' \\ \mathbf{D} \end{pmatrix} = \begin{pmatrix} \mathbf{A}^{-1}\mathbf{s}^{\mathrm{E}} & \mathbf{A}^{-1}\tilde{\mathbf{d}} \\ \mathbf{dB} & \boldsymbol{\varepsilon}^{\mathrm{T}} \end{pmatrix} \begin{pmatrix} \mathbf{T}' \\ \mathbf{E} \end{pmatrix}. \tag{2}$$

Here, $\mathbf{S}'$ and $\mathbf{T}'$ are the matrices of strains and stresses in $r\theta z$ coordinates; $\mathbf{A}$ and $\mathbf{B}$ are their corresponding second-order tensor transformation matrices.

In this study, we consider the outer and inner surfaces of the fiber to be free and the centrifugal and Coriolis forces are neglected in vibration. Thus, the stresses with respect to the radial direction can be ignored, because $T_r = T_{rz} = T_{r\theta} = 0$. While the helical electrodes act as equipotential layers among the fiber, the electric field in the 1 direction is significantly suppressed. On the assumption of uniform electric field, the electric field is considered as a pure helical form parallel to the 3 direction, as $E_1 = E_2 = 0$. Therefore, the relevant constitutive relations of the fiber are simplified as:

$$S_\theta = s^{\mathrm{E}}_{\theta\theta} T_\theta + s^{\mathrm{E}}_{\theta z} T_z + s^{\mathrm{E}}_{\theta\theta z} T_{\theta z} + d_{3\theta} E_3, \tag{3a}$$

$$S_{\theta z} = s^{\mathrm{E}}_{\theta\theta z} T_\theta + s^{\mathrm{E}}_{z\theta z} T_z + s^{\mathrm{E}}_{\theta z\theta z} T_{\theta z} + d_{3\theta z} E_3, \tag{3b}$$

$$S_z = s^{\mathrm{E}}_{\theta z} T_\theta + s^{\mathrm{E}}_{zz} T_z + s^{\mathrm{E}}_{z\theta z} T_{\theta z} + d_{3z} E_3, \tag{3c}$$

$$D_1 = d_{1\theta} T_\theta + d_{1z} T_z + d_{1\theta z} T_{\theta z}, \tag{3d}$$

$$D_3 = d_{3\theta} T_\theta + d_{3z} T_z + d_{3\theta z} T_{\theta z} + \varepsilon^{\mathrm{T}}_{33} E_3. \tag{3e}$$

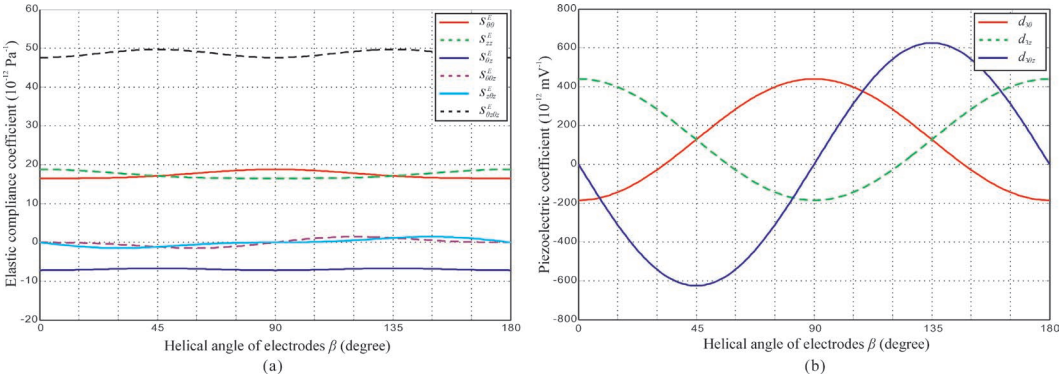

Fig. 3. Elastic compliance coefficients and piezoelectric coefficients as a function of β.

Compared with the original piezoelectric equations, these expressions are more straightforward for the description and analysis of the fiber. The desired piezoelectric coefficients and elastic compliance coefficients can be defined from the original material parameters and used directly to determine the state of the fiber under electric excitation and mechanical loads. Unlike the traditional piezoelectric d_{33} (or d_{31}) normal and d_{15} shear element, normal and shear strains (stresses) are coupled in this case, because electric excitation and mechanical loads generate torsional, longitudinal and tangential deformations of the fiber simultaneously. Stresses (strains) in θz coordinates have shear components in 13 coordinates and induce a nonzero electric displacement in the 1 direction, which indicates a non-uniform distribution of charge on the electrodes without changing the amount and sign of total charges.

Taking the typical piezoceramic material PZT-5A1 (Smart Materials Co., Sarasota, FL) as an example, the changing trends of elastic compliance coefficients and piezoelectric coefficients as functions of electric field orientation are investigated. The material properties of PZT-5A1 are listed in Table I. Fig. 3(a) shows the variation of elastic compliance coefficients for values of the electrode helical angle β from 0 to 180°. The elastic compliance coefficients fluctuate slightly around their original values. The intensities of these fluctuations are mainly determined by the elastic anisotropy of the material. The piezoelectric coefficients are strong functions of β in Fig. 3(b). Piezoelectric torsional strain reaches the highest value when $\beta = 45°$ (or 135°), with coefficient $d_{3\theta z}$ comparable to the d_{15} coefficient. The longitudinal deformation is weakened because of the opposite effects of the d_{33} and d_{31} coefficients. The fiber produces a zero longitudinal displacement if a suitable electrode helical angle is chosen ($\beta = 57.4°$ or 122.6°).

TABLE I. Material Data for PZT-5A1.

Symbol	Value	Unit
d_{33}	440	10^{-12} m V^{-1}
d_{31}	−185	10^{-12} m V^{-1}
d_{15}	560	10^{-12} m V^{-1}
ρ	7750	kg m^{-3}
$\varepsilon_1{}^{\mathrm{T}}/\varepsilon_0$	1660	—
$\varepsilon_3{}^{\mathrm{T}}/\varepsilon_0$	2004	—
$s_{11}{}^{\mathrm{E}}$	16.5	10^{-12} Pa^{-1}
$s_{12}{}^{\mathrm{E}}$	−5.8	10^{-12} Pa^{-1}
$s_{13}{}^{\mathrm{E}}$	−7.2	10^{-12} Pa^{-1}
$s_{33}{}^{\mathrm{E}}$	18.8	10^{-12} Pa^{-1}
$s_{44}{}^{\mathrm{E}}$	47.6	10^{-12} Pa^{-1}
$s_{66}{}^{\mathrm{E}}$	47.6	10^{-12} Pa^{-1}

III. Formulation of the Coupled Vibrations

The piezoelectric fiber with coupled torsional and longitudinal vibrations is shown in Fig. 4. M_1, M_2, F_1 and F_2 are the external torques and forces acting on the two ends of the fiber; φ_1, φ_2, u_{z1}, and u_{z2} are the torsional and longitudinal displacements at the ends (a dot over a variable denotes its corresponding velocity). In most cases, three kinds of basic boundary conditions are used: 1) free at two ends, 2) fixed at one end and free at another end, and 3) fixed at both ends. We analyze the vibration characteristics under the condition that the fiber is free at the two ends, as:

$$M_1 = M_2 = 0, \quad F_1 = F_2 = 0. \tag{4}$$

In the previous study [22], the electric field E_3 was considered constant under the assumption that the distance between adjacent electrodes was not large. The intensity of E_3 is expressed as

$$E_3 = \frac{V}{\pi r_{\mathrm{o}} \sin\beta}, \tag{5}$$

where V is the applied voltage. However, this assumption will influence the accuracy of the model in the resonant modes. Because of the electric continuity of piezoelectric material, electric parameters between the adjacent electrodes satisfy:

$$\frac{\partial D_3}{\partial 3} = 0, \quad \frac{\partial E_3}{\partial 1} = 0. \tag{6}$$

From (3e), the non-uniform distribution of stresses in the 3 direction clearly results in a distorted distribution of E_3

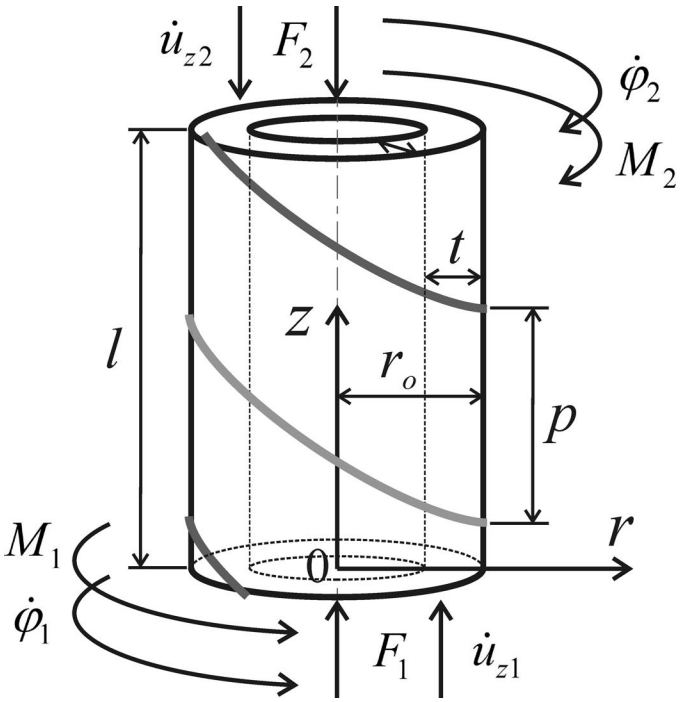

Fig. 4. Geometrical diagram and boundary condition of the fiber in coupled vibrations.

around its average value in (5). The variation of E_3 in the 3 direction indicates its variations in the θ and z directions and also changes other parameters. As mentioned above, the influences caused by the variations of relevant parameters in the θ direction are ignored to making a resoluble model, but their influences in the z direction are reserved.

We define n_1 and n_2 as the mechanical coupling coefficients between the stresses and let

$$T_\theta = n_1 T_{\theta z} + T'_\theta, \quad T_z = n_2 T_{\theta z}, \tag{7}$$

where $T_\theta{}'$ are independent parts with no respect to the position of the fiber. From (3e), (6), (7) and the assumption of $\partial T/\partial\theta = 0$, we obtain that the distribution of the stresses and electric field in the z direction satisfies the condition

$$\frac{\partial E_3}{\partial z} = -\frac{(n_1 d_{3\theta} + n_2 d_{3z} + d_{3\theta z})\cos^2\beta}{\varepsilon_{33}^{\mathrm{T}}}\frac{\partial T_{\theta z}}{\partial z} = g'\frac{\partial T_{\theta z}}{\partial z}. \tag{8}$$

Because of the assumptions regarding parameters in the r and θ directions, the 3-D motion equations and the relationships between strains and displacements for the piezoelectric fiber in $r\theta z$ cylindrical coordinates are [7]

$$\rho\frac{\partial^2 u_r}{\partial t^2} = -\frac{T_\theta}{r}, \quad \rho\frac{\partial^2 u_\theta}{\partial t^2} = \frac{\partial T_{\theta z}}{\partial z}, \quad \rho\frac{\partial^2 u_z}{\partial t^2} = \frac{\partial T_z}{\partial z}, \tag{9a}$$

$$S_\theta = \frac{u_r}{r}, \quad S_{\theta z} = \frac{\partial u_\theta}{\partial z}, \quad S_z = \frac{\partial u_z}{\partial z}. \tag{9b}$$

In the coupled torsional and longitudinal vibrations of the fiber, radial vibration also exists but in a different style.

For the simple harmonic motion with frequency ω, we define the applied voltage $V = V_a\exp(\mathrm{j}\omega t)$ and the displacements $u = u_a\exp(\mathrm{j}\omega t)$. Considering the radial displacement, we obtain the result that tangential strain and stress satisfy the condition

$$T_\theta = \rho\omega^2 r_{\mathrm{o}}^2 S_\theta. \tag{10}$$

Substituting (7) and (10) into (3a) yields

$$\begin{aligned}&\left[n_1\left(s_{\theta\theta}^{\mathrm{E}} - \frac{1}{\rho\omega^2 r_{\mathrm{o}}^2}\right) + n_2 s_{\theta z}^{\mathrm{E}} + s_{\theta\theta z}^{\mathrm{E}}\right]T_{\theta z}\\ &\quad + \left(s_{\theta\theta}^{\mathrm{E}} - \frac{1}{\rho\omega^2 r_{\mathrm{o}}^2}\right)T'_\theta + d_{3\theta}E_3 = 0.\end{aligned} \tag{11}$$

In the coupled vibrations, $T_{\theta z}$ has a large variation but $T_\theta{}'$ and E_3 are relatively constant, so we approximately obtain

$$n_1\left(s_{\theta\theta}^{\mathrm{E}} - \frac{1}{\rho\omega^2 r_{\mathrm{o}}^2}\right) + n_2 s_{\theta z}^{\mathrm{E}} + s_{\theta\theta z}^{\mathrm{E}} = 0, \tag{12a}$$

$$T'_\theta = \frac{d_{3\theta}}{\frac{1}{\rho\omega^2 r_{\mathrm{o}}^2} - s_{\theta\theta}^{\mathrm{E}}}E_3 = e'E_3, \tag{12b}$$

which indicate a coupling relation of stresses and the effect of $T_\theta{}'$ for the radial vibration.

From (3b), (3c), and (7), the distributions of shear and longitudinal strains and stresses in the z direction satisfy the equations

$$\frac{\partial S_{\theta z}}{\partial z} = (n_1 s_{\theta\theta z}^{\mathrm{E}} + n_2 s_{z\theta z}^{\mathrm{E}} + s_{\theta z\theta z}^{\mathrm{E}} + d_{3\theta z}g')\frac{\partial T_{\theta z}}{\partial z} = s_{\theta z\theta z}\frac{\partial T_{\theta z}}{\partial z}, \tag{13a}$$

$$\frac{\partial S_z}{\partial z} = \frac{1}{n_2}(n_1 s_{\theta z}^{\mathrm{E}} + n_2 s_{zz}^{\mathrm{E}} + s_{z\theta z}^{\mathrm{E}} + d_{3z}g')\frac{\partial T_z}{\partial z} = s_{zz}\frac{\partial T_z}{\partial z}, \tag{13b}$$

where $s_{\theta z\theta z}$ and s_{zz} are the modified shear and longitudinal elastic compliance coefficients including the piezoelectric effect and vibration coupling. Substituting (9b) and (13) into (9a), the governing equations for the torsional and longitudinal vibrations are

$$\frac{d^2 u_\theta}{dz^2} + k_{\theta z}^2 u_\theta = 0, \tag{14a}$$

$$\frac{d^2 u_z}{dz^2} + k_z^2 u_z = 0, \tag{14b}$$

where $k_{\theta z} = \omega(\rho \cdot s_{\theta z\theta z})^{1/2}$ is the torsional wave number and $k_z = \omega(\rho \cdot s_{zz})^{1/2}$ is the longitudinal wave number. The solutions of (14) are

$$u_\theta = A_{\theta z}\sin k_{\theta z}z + B_{\theta z}\cos k_{\theta z}z, \tag{15a}$$

$$u_z = A_z \sin k_z z + B_z \cos k_z z, \tag{15b}$$

where A and B are determined by the boundary condition of the fiber in Fig. 4. The tangential and longitudinal vibrations at the two ends of the fiber are defined as

$$u_{\theta(0)} = u_{\theta 1} = r_o \varphi_1, \quad u_{\theta(l)} = -u_{\theta 2} = -r_o \varphi_2, \tag{16a}$$

$$u_{z(0)} = u_{z1}, \quad u_{z(l)} = -u_{z2}. \tag{16b}$$

Then, the torsional and longitudinal displacements of the fiber are deduced as

$$\varphi = \frac{\varphi_1 \sin k_{\theta z}(l-z) - \varphi_2 \sin k_{\theta z} z}{\sin k_{\theta z} l}, \tag{17a}$$

$$u_z = \frac{u_{z1} \sin k_z (l-z) - u_{z2} \sin k_z z}{\sin k_z l}. \tag{17b}$$

The strains, stresses, longitudinal force, and torque can also be calculated.

From (3), (5), and (10), the electric displacement D_3 can be expressed by the parameters $T_{\theta z}$, T_z, and E_3. Then with (16) and (17), the charge of electrodes Q is calculated from the integration of D_3, and the current is obtained using $I = j\omega Q$. The equivalent admittance of the fiber in the coupled vibrations is given as

$$\begin{aligned} Y = \frac{j\omega Q}{V} = j\omega \frac{2tl\varepsilon_{33}^{\mathrm{T}}}{\pi r_o \sin^2 \beta} \Bigg[& 1 + \frac{(d_{3\theta z} + e' s_{\theta\theta z}^{\mathrm{E}})^2 \tan \frac{k_{\theta z} l}{2}}{\varepsilon_{33}^{\mathrm{T}} s_{\theta z \theta z}^{\mathrm{E}\prime} \frac{k_{\theta z} l}{2}} \\ & + \frac{(d_{3z} + e' s_{\theta z}^{\mathrm{E}})^2 \tan \frac{k_z l}{2}}{\varepsilon_{33}^{\mathrm{T}} s_{zz}^{\mathrm{E}\prime} \frac{k_z l}{2}} + \frac{e' d_{3\theta}}{\varepsilon_{33}^{T}} - \frac{(d_{3\theta z} + e' s_{\theta\theta z}^{\mathrm{E}})^2}{\varepsilon_{33}^{\mathrm{T}} s_{\theta z \theta z}^{\mathrm{E}\prime}} \\ & - \frac{(d_{3z} + e' s_{\theta z}^{\mathrm{E}})^2}{\varepsilon_{33}^{\mathrm{T}} s_{zz}^{\mathrm{E}\prime}} \Bigg], \end{aligned} \tag{18}$$

where

$$s_{\theta z \theta z}^{\mathrm{E}\prime} = n_1 s_{\theta\theta z}^{\mathrm{E}} + n_2 s_{z\theta z}^{\mathrm{E}} + s_{\theta z \theta z}^{\mathrm{E}},$$

$$s_{zz}^{\mathrm{E}\prime} = \frac{1}{n_2}(n_1 s_{\theta z}^{\mathrm{E}} + n_2 s_{zz}^{\mathrm{E}} + s_{z\theta z}^{\mathrm{E}}).$$

From this deduction, the equivalent circuit of the piezoelectric fiber in coupled vibration can also be described in Fig. 5.

IV. Numerical Analyses and Experiments

For a piezoelectric fiber vibrating in the coupled resonant modes, the admittance Y in (18) has the maximal value. Therefore, the frequency equations in the coupled vibrations are given as

$$k_{\theta z} l = k_z l = (2n-1)\pi, \quad n = 1, 2, 3, \ldots. \tag{19}$$

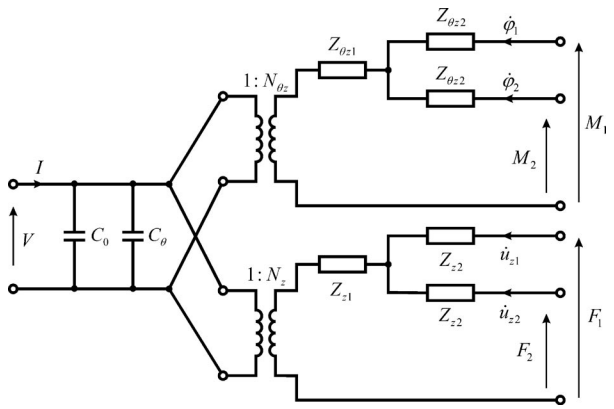

Fig. 5. Equivalent circuits of the piezoelectric fiber actuator in coupled vibrations.

Given the material parameters and geometrical dimensions of the fiber, the resonant frequencies and mechanical coupling coefficients can be calculated from (11b) and (19).

With help of the mathematical software MatLab (The MathWorks Inc., Natick, MA), numerical methods are used to find the solutions of the frequency equations. For PZT-5A1 fibers with a radius r_o of 0.5 mm, the solutions are investigated as functions of the electrode helical angle β and fiber length l. From the computed results, two groups of solutions are found for the first-order coupled vibration: f_{T}, $n_{1\mathrm{T}}$, and $n_{2\mathrm{T}}$ for coupled torsional vibration mode; f_{L}, $n_{1\mathrm{L}}$, and $n_{2\mathrm{L}}$ for coupled longitudinal vibration mode ($f_{\mathrm{T}} < f_{\mathrm{L}}$). Figs. 6(a) and 6(c) show the resonant frequencies f_{T} and f_{L} as functions of electrode helical angle β and fiber length l. Figs. 6(b) and 6(d) show the corresponding trends of mechanical coupling coefficients. Here, $n_{1\mathrm{T}}$ and $n_{2\mathrm{T}}$ denote the relative intensity of coupled tangential and longitudinal stresses in the torsional mode; $n_{1\mathrm{L}}/n_{2\mathrm{L}}$ and $1/n_{2\mathrm{L}}$ denote the relative intensity of coupled tangential and torsional stresses in the longitudinal mode. For constant fiber length (50 mm), f_{T} fluctuates with electrode helical angle β, and we obtain the highest value when $\beta = 35°$. f_{L} shows a large change for $\beta < 45°$, and tends toward a constant with $\beta > 45°$. $n_{2\mathrm{T}}$ and $1/n_{2\mathrm{L}}$ have the same absolute value but with inverse signs. A large coupling of torsional and longitudinal stresses occurs with β around 25°. The coupled tangential stresses are weak in both torsional and longitudinal vibration modes, which can actually be ignored. When β tends to zero, the fiber can be regarded as a small piezoelectric stack; and when β is equal to 90°, the fiber is polarized and driven with a tangential electric field. In these two special cases, the couplings between torsional and longitudinal stresses are zero, and only longitudinal deformation is realized. When $\beta = 50.7°$, another zero coupling point occurs. However, this point is different from the static longitudinal zero point ($\beta = 57.4°$). For constant electrode helical angle ($\beta = 30°$), f_{T} and f_{L} are both inversely proportional to the fiber length l when $l > 15$ mm, and $n_{2\mathrm{T}}$ and $1/n_{2\mathrm{L}}$ are nearly constant. However, for $l < 15$ mm, the coupling between longitudinal and tangential stresses has a remarkable improvement and

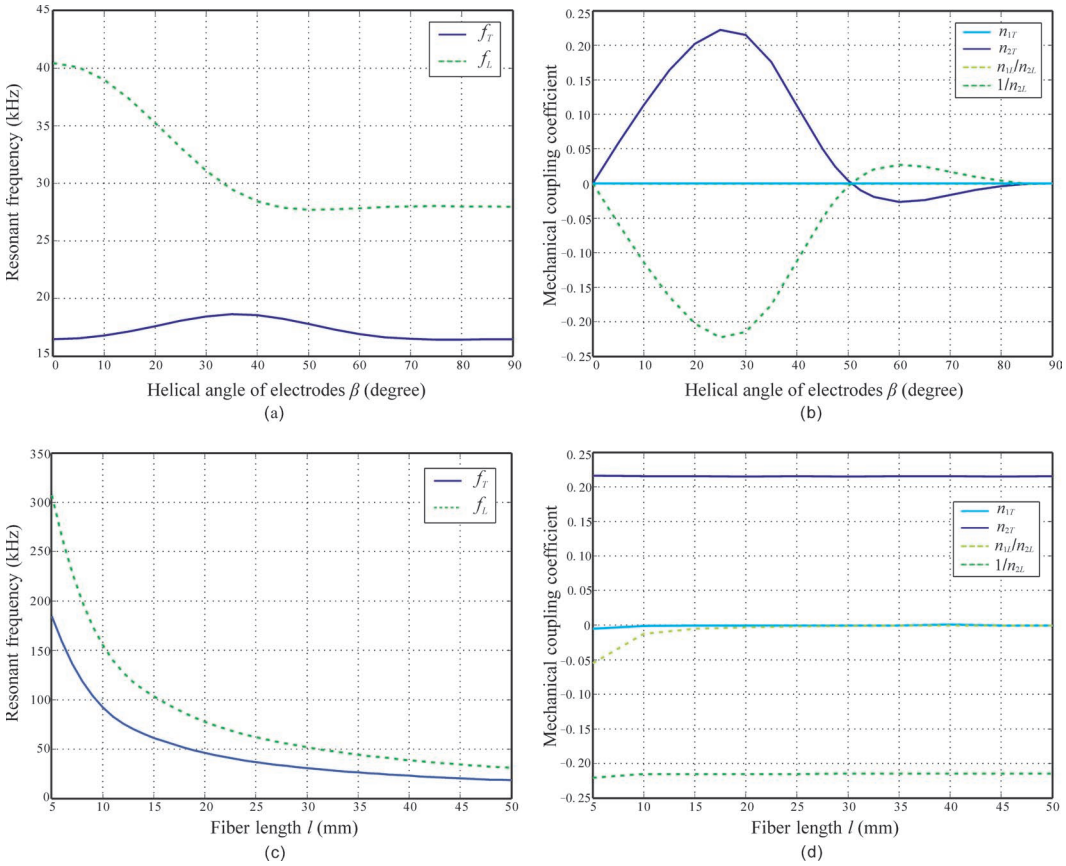

Fig. 6. (a) Resonant frequencies as a function of β, (b) mechanical coupling coefficients as the function of β ($l = 50$ mm), (c) resonant frequencies as the functions of l, and (d) mechanical coupling coefficients as the function of l ($\beta = 30°$).

influence on the resonant frequency of the longitudinal mode. For a fiber with length comparable to its radius, it becomes a cylinder similar to that described in [21].

Resonant frequencies of several samples are measured to verify the proposed analyses. The samples are made of tubular PZT-5A1 fibers (Smart Materials Co., Sarasota, FL) with outer radius r_o of 0.5 mm and wall thickness t of 0.2 mm. Two pieces of copper wire with a diameter of 40 μm are used as electrodes and wrapped around the outer surface of fibers with a pitch from1 mm to 5 mm. Epoxy adhesive (DP460) with a thickness of around 20 μm is used to attach the electrodes onto the fiber surface for fixation and insulation. Finally, samples are polarized in thermostatic silicone oil at 80°C with an effective electric field intensity of 2000 V·mm^{-1}, lasting for 20 min. The finished samples have a uniform length of 50 mm with electrodes along the entire length of the fibers.

The frequency characteristics of the finished samples are measured with a precision impedance analyzer (GW8101, Good Will Instrument Co., New Taipei City, Taiwan) and corresponding resonant frequencies are extracted. Fig. 7 shows a typical admittance characteristic of the sample in free-free boundary condition. The resonant frequencies of first-order torsional and longitudinal vibrations are approximately 19.2 and 29.8 kHz, respectively. The high-order vibration modes can also be found, such as the third-order torsional mode at 58.3 kHz, the

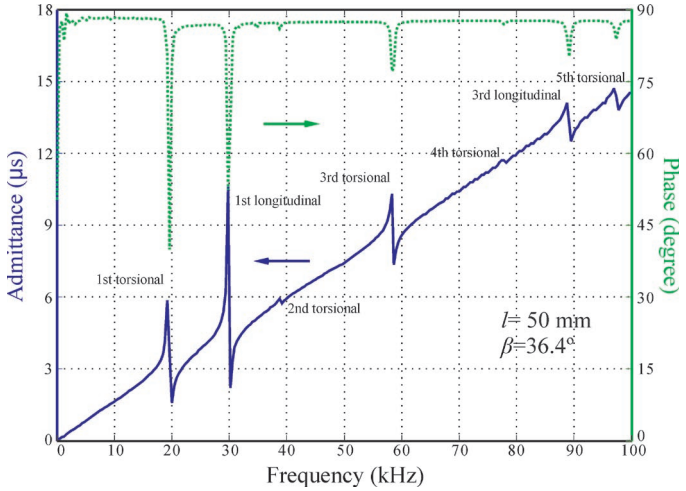

Fig. 7. Typical frequency characteristics of a sample with free-free boundary condition.

third-order longitudinal mode at 88.7 kHz, and the fifth-order torsional mode at 95.9 kHz. The frequencies of the third-order and fifth-order modes are approximately three and five times the values of the first-order mode, which is consistent with the theoretical analyses. Two unremarkable modes at 38.8 and 77.6 kHz, which considered as the second-order and fourth-order modes of torsional vibrations, can be found in the admittance curve. They are not

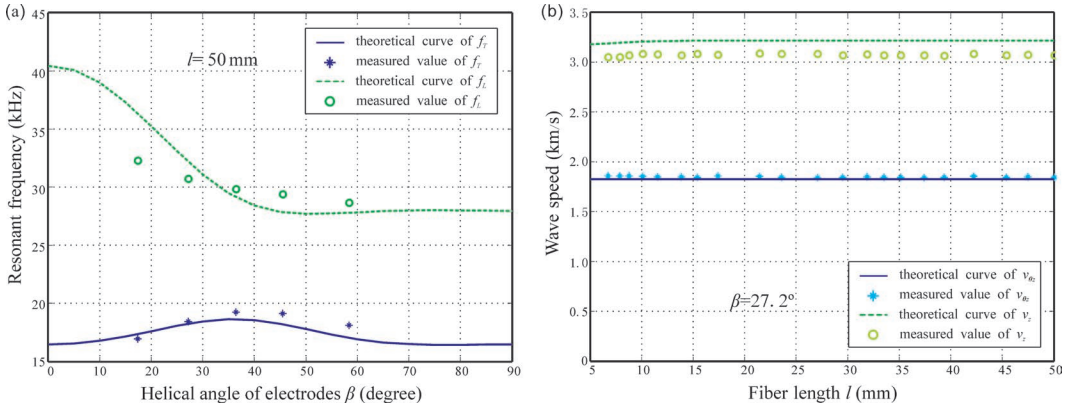

Fig. 8. (a) Measured resonant frequencies as a function of β ($l = 50$ mm), (b) measured wave speeds as a function of l ($\beta = 27.2°$).

expected for the fiber under electric excitation in theory, but result from the non-uniformity of the fiber and handmade electrodes.

Fig. 8(a) shows the experimental results of first-order f_T and f_L with different electrode helical angles β. The results show the same trend as theoretical curves, but there are clear discrepancies between theoretical and measured values. We consider three possible reasons for such discrepancies: 1) discrepancy between the actual and given material parameters, 2) imperfect polarization of the fibers, and 3) discrepancy between the simplified model and practical samples. The latter two are considered to be the primary reasons. First, the surface helical electrodes induce a nonuniform distribution of electric field between adjacent electrodes [16]. The polarization electric field contorts severely near the electrodes (called the dead zone). Material in a dead zone will have an inefficient polarization and lead to discrepancies from the actual material parameters. Moreover, the pattern of the electric field is also distorted near the ends of the fiber. Second, the theoretical model simplifies the variations of relevant parameters in the radial and tangential directions, which also results in discrepancies between the theoretical model and actual samples. The electric field angle changes in the radial direction and influences the material parameters of the fiber [16]. The ignored variations of relevant parameters in the θ direction will weaken the changes of the modified elastic compliance coefficients $s_{\theta z\theta z}$ and s_{zz}, which have direct relations for the resonant frequencies. Fig. 8(b) shows the experimental results of torsional and longitudinal wave speeds $v = 2f_r l$ as functions of fiber length. The change trends of both wave speeds agree well with the theoretical curves.

V. Conclusion

An improved dynamic model was developed to describe the complex coupled torsional and longitudinal vibrations of piezoelectric fiber with helical electrodes. Equivalent circuits of the coupled vibrations were also obtained. Numerical analyses showed that the coupled torsional and longitudinal resonant frequencies are functions of electrode helical angle and fiber length. Their mechanical coupling coefficients can be optimized with the proper electrode helical angle. The trends of the calculated resonant frequencies were validated with experimental results. We believe that this work provides a useful reference for the optimization of the piezoelectric fiber in practice and a significant attempt to investigate the characteristics of such kinds of piezoelectric elements.

Appendix

The second-order tensor transformation matrices **A** and **B** in (2) are shown in Eqs. (A-1a) and (A-1b), see next page. The full constitutive relations of the fiber in (3) are

$$\begin{aligned} S_\theta &= [s_{11}^{\mathrm{E}}\cos^4\beta + s_{33}^{\mathrm{E}}\sin^4\beta + (2s_{13}^{\mathrm{E}} + s_{44}^{\mathrm{E}})\sin^2\beta\cos^2\beta]T_\theta \\ &\quad + [(s_{11}^{\mathrm{E}} + s_{33}^{\mathrm{E}} - s_{44}^{\mathrm{E}})\sin^2\beta\cos^2\beta + s_{13}^{\mathrm{E}}(\sin^4\beta + \cos^4\beta)]T_z \\ &\quad + \{[2(s_{11}^{\mathrm{E}} - s_{13}^{\mathrm{E}})\cos^2\beta + 2(s_{13}^{\mathrm{E}} - s_{33}^{\mathrm{E}})\sin^2\beta \\ &\quad + s_{44}^{\mathrm{E}}(\sin^2\beta - \cos^2\beta)]\sin\beta\cos\beta\}T_{\theta z} \\ &\quad + (d_{31}\cos^2\beta + d_{33}\sin^2\beta)E_3, \end{aligned} \tag{A-2a}$$

$$\begin{aligned} S_z &= [s_{13}^{\mathrm{E}}(\cos^4\beta + \sin^4\beta) + (s_{11}^{\mathrm{E}} + s_{33}^{\mathrm{E}} - s_{44}^{\mathrm{E}})\sin^2\beta\cos^2\beta]T_\theta \\ &\quad + [s_{11}^{\mathrm{E}}\sin^4\beta + s_{33}^{\mathrm{E}}\cos^4\beta + (2s_{13}^{\mathrm{E}} + s_{44}^{\mathrm{E}})\sin^2\beta\cos^2\beta]T_z \\ &\quad + \{[2(s_{11}^{\mathrm{E}} - s_{13}^{\mathrm{E}})\sin^2\beta + 2(s_{13}^{\mathrm{E}} - s_{33}^{\mathrm{E}})\cos^2\beta \\ &\quad - s_{44}^{\mathrm{E}}(\sin^2\beta - \cos^2\beta)]\sin\beta\cos\beta\}T_{\theta z} \\ &\quad + (d_{31}\sin^2\beta + d_{33}\cos^2\beta)E_3, \end{aligned} \tag{A-2b}$$

$$\begin{aligned} S_{\theta z} &= \{[2(s_{11}^{\mathrm{E}} - s_{13}^{\mathrm{E}})\cos^2\beta + 2(s_{13}^{\mathrm{E}} - s_{33}^{\mathrm{E}})\sin^2\beta \\ &\quad + (\sin^2\beta - \cos^2\beta)]\sin\beta\cos\beta\}T_\theta \\ &\quad + \{[2(s_{11}^{\mathrm{E}} - s_{13}^{\mathrm{E}})\sin^2\beta + 2(s_{13}^{\mathrm{E}} - s_{33}^{\mathrm{E}})\cos^2\beta \\ &\quad - s_{44}^{\mathrm{E}}(\sin^2\beta - \cos^2\beta)]\sin\beta\cos\beta\}T_z \\ &\quad + [4(s_{11}^{\mathrm{E}} - 2s_{13}^{\mathrm{E}} + s_{33}{}^{\mathrm{E}})\sin^2\beta\cos^2\beta \\ &\quad + s_{44}^{\mathrm{E}}(\sin^2\beta - \cos^2\beta)^2]T_{\theta z} + [2(d_{31} - d_{33})\sin\beta\cos\beta]E_3 \end{aligned} \tag{A-2c}$$

$$\begin{aligned} D_1 &= d_{15}T_\theta\sin\beta\cos\beta - d_{15}T_z\sin\beta\cos\beta \\ &\quad + d_{15}(\sin^2\beta - \cos^2\beta)T_{\theta z}, \end{aligned} \tag{A-2d}$$

$$\mathbf{A} = \begin{bmatrix} 0 & \cos^2\beta & \sin^2\beta & \sin\beta\cos\beta & 0 & 0 \\ 1 & 0 & 0 & 0 & 0 & 0 \\ 0 & \sin^2\beta & \cos^2\beta & -\sin\beta\cos\beta & 0 & 0 \\ 0 & 0 & 0 & 0 & -\cos\beta & \sin\beta \\ 0 & 2\sin\beta\cos\beta & -2\sin\beta\cos\beta & \sin^2\beta - \cos^2\beta & 0 & 0 \\ 0 & 0 & 0 & 0 & \sin\beta & \cos\beta \end{bmatrix} \tag{A-1a}$$

$$\mathbf{B} = \begin{bmatrix} 0 & \cos^2\beta & \sin^2\beta & 2\sin\beta\cos\beta & 0 & 0 \\ 1 & 0 & 0 & 0 & 0 & 0 \\ 0 & \sin^2\beta & \cos^2\beta & -2\sin\beta\cos\beta & 0 & 0 \\ 0 & 0 & 0 & 0 & -\cos\beta & \sin\beta \\ 0 & \sin\beta\cos\beta & -\sin\beta\cos\beta & \sin^2\beta - \cos^2\beta & 0 & 0 \\ 0 & 0 & 0 & 0 & \sin\beta & \cos\beta \end{bmatrix} \tag{A-1b}$$

$$D_3 = (d_{31}\cos^2\beta + d_{33}\sin^2\beta)T_\theta + (d_{31}\sin^2\beta + d_{33}\cos^2\beta)T_z + 2(d_{31} - d_{33})T_{\theta z}\sin\beta\cos\beta + \varepsilon_{33}^T E_3, \tag{A-2e}$$

$$S_r = (s_{12}^{\mathrm{E}}\cos^2\beta + s_{13}^{\mathrm{E}}\sin^2\beta)T_\theta + (s_{12}^{\mathrm{E}}\sin^2\beta + s_{13}^{\mathrm{E}}\cos^2\beta)T_z + [2(s_{12}^{\mathrm{E}} - s_{13}^{\mathrm{E}})\sin\beta\cos\beta]T_{\theta z} + d_{31}E_3, \tag{A-2f}$$

$$S_{rz} = s_{r\theta} = D_2 = 0. \tag{A-2g}$$

The strains, stresses, longitudinal force, and torque of the fiber calculated from (17) are

$$S_{\theta z} = \frac{-r_{\mathrm{o}}\varphi_1 k_{\theta z}\cos k_{\theta z}(l-z) - r_{\mathrm{o}}\varphi_2 k_{\theta z}\cos k_{\theta z} z}{\sin k_{\theta z} l}, \tag{A-3a}$$

$$S_z = \frac{du_z}{dz} = \frac{-u_{z1}k_z\cos k_z(l-z) - u_{z2}k_z\cos k_z z}{\sin k_z l}, \tag{A-3b}$$

$$T_{\theta z} = \frac{1}{s_{\theta z\theta z}^{\mathrm{E}\prime}} S_{\theta z} - \frac{1}{s_{\theta z\theta z}^{\mathrm{E}\prime}}(e' s_{\theta\theta z}^{\mathrm{E}} + d_{3\theta z})E_3, \tag{A-3c}$$

$$T_z = \frac{1}{s_{zz}^{\mathrm{E}\prime}} S_z - \frac{1}{s_{zz}^{\mathrm{E}\prime}}(e' s_{\theta z}^{\mathrm{E}} + d_{3z})E_3 \tag{A-3d}$$

$$M_z = T_{\theta z} r_{\mathrm{o}} S, \quad F_z = T_z S, \tag{A-3e}$$

where $S = 2\pi r_{\mathrm{o}} t$ is the cross-section of the fiber.

The longitudinal forces and torques at the two ends of the fiber and current I, which was used to determine the equivalent circuits of the fiber in coupled vibration, are expressed as

$$\begin{aligned} M_1 &= -T_{\theta z(0)} r_{\mathrm{o}} S = \frac{k_{\theta z} r_{\mathrm{o}}^2 S}{j\omega s_{\theta z\theta z}^{\mathrm{E}\prime}\sin k_{\theta z} l}(\dot\varphi_1 + \dot\varphi_2) \\ &\quad + \frac{j k_{\theta z} r_{\mathrm{o}}^2 S}{\omega s_{\theta z\theta z}^{\mathrm{E}\prime}}\left(\tan\frac{k_{\theta z} l}{2}\right)\dot\varphi_1 + \frac{2t r_{\mathrm{o}}(d_{3\theta z} + e' s_{\theta\theta z}^{\mathrm{E}})}{s_{\theta z\theta z}^{\mathrm{E}\prime}\sin\beta} V \\ &= Z_{\theta z1}(\dot\varphi_1 + \dot\varphi_2) + Z_{\theta z2}\dot\varphi_1 + N_{\theta z} V, \end{aligned} \tag{A-4a}$$

$$\begin{aligned} M_2 &= -T_{\theta z(0)} r_{\mathrm{o}} S = \frac{k_{\theta z} r_{\mathrm{o}}^2 S}{j\omega s_{\theta z\theta z}^{\mathrm{E}\prime}\sin k_{\theta z} l}(\dot\varphi_1 + \dot\varphi_2) \\ &\quad + \frac{j k_{\theta z} r_{\mathrm{o}}^2 S}{\omega s_{\theta z\theta z}^{\mathrm{E}\prime}}\left(\tan\frac{k_{\theta z} l}{2}\right)\dot\varphi_2 + \frac{2t r_{\mathrm{o}}(d_{3\theta z} + e' s_{\theta\theta z}^{\mathrm{E}})}{s_{\theta z\theta z}^{\mathrm{E}\prime}\sin\beta} V \\ &= Z_{\theta z1}(\dot\varphi_1 + \dot\varphi_2) + Z_{\theta z2}\dot\varphi_2 + N_{\theta z} V, \end{aligned} \tag{A-4b}$$

$$\begin{aligned} F_1 &= -T_{z(0)} S = \frac{k_z S}{j\omega s_{zz}^{\mathrm{E}\prime}\sin k_z l}(\dot u_{z1} + \dot u_{z2}) \\ &\quad + \frac{j k_z S}{\omega s_{zz}^{\mathrm{E}\prime}\sin k_z l}\left(\tan\frac{k_z l}{2}\right)\dot u_{z1} + \frac{2t(d_{3z} + e' s_{\theta z}^{\mathrm{E}})}{s_{zz}^{\mathrm{E}\prime}\sin\beta} V \\ &= Z_{z1}(\dot u_{z1} + \dot u_{z2}) + Z_{z2}\dot u_{z1} + N_z V, \end{aligned} \tag{A-4c}$$

$$\begin{aligned} F_2 &= -T_{z(l)} S = \frac{k_z S}{j\omega s_{zz}^{\mathrm{E}\prime}\sin k_z l}(\dot u_{z1} + \dot u_{z2}) \\ &\quad + \frac{j k_z S}{\omega s_{zz}^{\mathrm{E}\prime}\sin k_z l}\left(\tan\frac{k_z l}{2}\right)\dot u_{z2} + \frac{2t(d_{3z} + e' s_{\theta z}^{\mathrm{E}})}{s_{zz}^{\mathrm{E}\prime}\sin\beta} V \\ &= Z_{z1}(\dot u_{z1} + \dot u_{z2}) + Z_{z2}\dot u_{z2} + N_z V, \end{aligned} \tag{A-4d}$$

$$I = j\omega \frac{2tl\varepsilon_{33}^{T}}{\pi r_{\mathrm{o}} \sin^2 \beta} V + j\omega \left[\frac{s' d_{3\theta}}{\varepsilon_{33}^{T}} - \frac{(d_{3\theta z} + e' s_{\theta\theta z}^{\mathrm{E}})^2}{\varepsilon_{33}^{\mathrm{T}} s_{\theta z\theta z}^{\mathbf{E}\prime}} - \frac{(d_{3z} + e' s_{\theta z}^{\mathrm{E}})^2}{\varepsilon_{33}^{\mathrm{T}} s_{zz}^{\mathrm{E}\prime}} \right] \frac{2tl\varepsilon_{33}^{\mathrm{T}}}{\pi r_{\mathrm{o}} \sin^2 \beta} V - \frac{2tr_{\mathrm{o}}(d_{3\theta z} + e' s_{\theta\theta z}^{\mathrm{E}})}{s_{\theta z\theta z}^{\mathrm{E}\prime} \sin \beta} (\dot{\varphi}_1 + \dot{\varphi}_2) - \frac{2t(d_{3z} + e' s_{\theta z}^{\mathrm{E}})}{s_{zz}^{\mathrm{E}\prime} \sin \beta} (\dot{u}_{z1} + \dot{u}_{z2}) = j\omega C_o V + j\omega C_\theta V - N_{\theta z}(\dot{\varphi}_1 + \dot{\varphi}_2) - N_z(\dot{u}_{z1} + \dot{u}_{z2}). \tag{A-4e}$$

References

[1] C. Niezrecki, D. Brei, S. Balakrishna, and A. Moskalik, "Piezoelectric actuation: State of the art," *Shock Vib. Dig.*, vol. 33, no. 4, pp. 269–280, 2001.

[2] J. F. Tressler, S. Alkoy, and R. E. Newnham, "Piezoelectric sensors and sensor materials," *J. Electroceram.*, vol. 2, no. 4, pp. 257–272, 1998.

[3] T. Kanda, A. Makino, T. Ono, K. Suzumori, T. Morita, and M. K. Kurosawa, "A micro ultrasonic motor using a micro-machined cylindrical bulk PZT transducer," *Sens. Actuators A*, vol. 127, no. 1, pp. 131–138, 2006.

[4] H. Zhang, S. X. Dong, S. Y. Zhang, T. H. Wang, Z. N. Zhang, and L. Fan, "Ultrasonic micro-motor using miniature piezoelectric tube with diameter of 1.0 mm," *Ultrasonics*, vol. 44, pp. e603–e606, 2006.

[5] J. S. Yang and H. Y. Fang, "A new ceramic tube piezoelectric gyroscope," *Sens. Actuators A*, vol. 107, no. 1, pp. 42–49, 2003.

[6] Y. Kagawa, N. Wakatsuki, T. Tsuchiya, and Y. Terada, "A tubular piezoelectric vibrator gyroscope," *IEEE Sensors J.*, vol. 6, no. 2, pp. 325–330, 2006.

[7] S. Y. Lin, "Study on the equivalent circuit and coupled vibration for the longitudinally polarized piezoelectric ceramic hollow cylinders," *J. Sound Vib.*, vol. 275, no. 3–5, pp. 859–875, 2004.

[8] J. O. Kim and J. G. Lee, "Dynamic characteristics of piezoelectric cylindrical transducers with radial polarization," *J. Sound Vib.*, vol. 300, no. 1–2, pp. 241–249, 2007.

[9] J. O. Kim and O. S. Kwon, "Vibration characteristics of piezoelectric torsional transducers," *J. Sound Vib.*, vol. 264, no. 2, pp. 453–473, 2003.

[10] S. Mishiro, "Torsional vibration apparatus," U.S. Patent 4652786, Mar. 24, 1987.

[11] S. Mishiro, "Torsion vibrator," U.S. Patent 4787265, Nov. 29, 1988.

[12] J. S. Yang, H. Y. Fang, and Q. Jiang, "A vibrating piezoelectric ceramic shell as a rotation sensor," *Smart Mater. Struct.*, vol. 9, no. 4, pp. 445–451, 2000.

[13] C. Kim, D. Lewis, III, C. C. Wu, A. Glazounov, and Q. M. Zhang, "High authority piezoelectric torsional actuators," in *11th IEEE Int. Symp. Applications Ferroelectrics*, 1998, pp. 277–280.

[14] T. Morita, R. Yoshida, Y. Okamoto, M. K. Kurosawa, and T. Higuchi, "A smooth impact rotation motor using a multi-layered torsional piezoelectric actuator," *IEEE Trans. Ultrason. Ferroelectr. Freq. Control*, vol. 46, no. 6, pp. 1439–1445, 1999.

[15] S. Vidoli and B. C. Batra, "Coupled extensional and torsional deformations of a piezoelectric cylinder," *Smart Mater. Struct.*, vol. 10, no. 2, pp. 300–304, 2001.

[16] C. L. Pan, Y. T. Ma, Y. B. Liu, Q. Zhang, and Z. H. Feng, "Torsional displacement of piezoelectric fiber actuators with helical electrodes," *Sens. Actuators A*, vol. 148, no. 1, pp. 250–258, 2008.

[17] W. X. Han, Q. Zhang, Y. T. Ma, C. L. Pan, and Z. H. Feng, "An impact rotary motor based on a fiber torsional piezoelectric actuator," *Rev. Sci. Instrum.*, vol. 80, no. 1, art. no. 014701, 2009.

[18] C. L. Pan, Y. T. Ma, J. Yin, F. R. Kong, and Z. H. Feng, "Miniature orthogonal optical scanning mirror excited by torsional piezoelectric fiber actuator," *Sens. Actuators A*, vol. 165, no. 2, pp. 329–337, Feb. 2011.

[19] A. Belloli, B. Castelli, X. Kornmann, C. Huber, and P. Ermanni, "Modeling and characterization of active fiber composites," *Proc. SPIE*, vol. 5390, pp. 78–88, 2004.

[20] D. J. Warkentin, "Modeling and electrode optimization for torsional IDE piezoceramics," *Proc. SPIE*, vol. 3985, pp. 840–854, 2000.

[21] Y. Fudaa and T. Yoshidaa, "Piezoelectric torsional actuator," *Ferroelectrics*, vol. 160, no. 1, pp. 323–330, 1994.

[22] L. M. Xu, F. Yang, Y. T. Hu, H. Fan, and J. S. Yang, "Vibration characteristics of a circular cylindrical ceramic tube piezoelectric transducer with helical electrodes," *IEEE Trans. Ultrason. Ferroelectr. Freq. Control*, vol. 56, no. 11, pp. 2587–2591, 2009.

Authors' photographs and biographies were unavailable at time of publication.